



Real-Time Spatial Registration for 3D Human Atlas

Lu Chen
Department of Computer Science,
Stony Brook University
Stony Brook, USA

Dejun Teng
School of Computer Science and
Technology, Shandong University
Qingdao, China

Tian Zhu
Department of Applied Mathematics
and Statistics, Stony Brook University
Stony Brook, USA

Jun Kong
Department of Mathematics and
Statistics, Georgia State University
Atlanta, USA

Bruce W. Herr II
Department of Intelligent Systems
Engineering, Luddy School of
Informatics, Computing, and
Engineering, Indiana University
Bloomington, USA

Andreas Bueckle
Department of Intelligent Systems
Engineering, Luddy School of
Informatics, Computing, and
Engineering, Indiana University
Bloomington, USA

Katy Börner
Department of Intelligent Systems
Engineering, Luddy School of
Informatics, Computing, and
Engineering, Indiana University
Bloomington, USA

Fusheng Wang
Department of Biomedical
Informatics and Department of
Computer Science, Stony Brook
University
Stony Brook, USA

ABSTRACT

The human body is made up of about 37 trillion cells (adults). Each cell has its own unique role and is affected by its neighboring cells and environment. The NIH Human BioMolecular Atlas Program (HuBMAP) aims at developing a 3D atlas of human body consisting of organs, vessels, tissues to single cells with all 3D spatially registered in a single 3D human atlas using tissues obtained from normal individuals across a wide range of ages. A critical step of building the atlas is to register 3D tissue blocks in real-time to the right location of a human organ, which itself consists of complex 3D substructures. The complexity of the 3D organ model, e.g., 35 meshes for a typical kidney, poses a significant computational challenge for the registration. In this paper, we propose a comprehensive framework TICKET (Tissue block rEgisTration) to support tissue block registration for 3D human atlas, including (1) 3D mesh pre-processing, (2) spatial queries on intersection relationship and (3) intersection volume computation between organs and tissue blocks. To minimize search space and computation cost, we develop multi-level indexing at both the anatomical structure level and mesh level, and utilize OpenMP for parallel computing. Considering cuboid based shape of the tissue block, we propose an efficient voxelization-based method to estimate the intersection volume. Our experiments demonstrate that the proposed framework is efficient and practical. TICKET is being integrated into the HuBMAP CCF registration portal [1].

Permission to make digital or hard copies of all or part of this work for personal or classroom use is granted without fee provided that copies are not made or distributed for profit or commercial advantage and that copies bear this notice and the full citation on the first page. Copyrights for components of this work owned by others than ACM must be honored. Abstracting with credit is permitted. To copy otherwise, or republish, to post on servers or to redistribute to lists, requires prior specific permission and/or a fee. Request permissions from permissions@acm.org.

BigSpatial '22, November 1, 2022, Seattle, WA, USA

© 2022 Association for Computing Machinery.

ACM ISBN 978-1-4503-9531-1/22/11...\$15.00

<https://doi.org/10.1145/3557917.3567618>

CCS CONCEPTS

• Information systems → 3D Data management systems.

KEYWORDS

3D Spatial Queries, Spatial Indexing, Parallel Computing, Human Atlas

ACM Reference Format:

Lu Chen, Dejun Teng, Tian Zhu, Jun Kong, Bruce W. Herr II, Andreas Bueckle, Katy Börner, and Fusheng Wang. 2022. Real-Time Spatial Registration for 3D Human Atlas. In *The 10th ACM SIGSPATIAL International Workshop on Analytics for Big Geospatial Data (BigSpatial '22) (BigSpatial '22)*, November 1, 2022, Seattle, WA, USA. ACM, Seattle, WA, USA, 9 pages. <https://doi.org/10.1145/3557917.3567618>

1 INTRODUCTION

With the significant development of tissue imaging technologies[2] [3] [4] [5], enormous amounts of information about our human body are now being produced at both cellular and subcellular levels. The human body, which consists of more than 70 organs and 37 trillion cells, can be viewed as a special atlas. Every organ and every cell have corresponding coordinates. The Human BioMolecular Atlas Program (HuBMAP) [6] of National Institutes of Health is a national initiative to develop an open, global framework for comprehensively mapping of the human body at cellular resolution, in particular, generating foundational 3D tissue atlases of human body, to better understand how the healthy human body works and what changes during aging or disease. A Human Body Common Coordinate Framework [7], encompassing 3D organization of whole organs and thousands of anatomical structures, are being built by HuBMAP, where the organs and the anatomical structures are represented in mesh based 3D models [8].

By collecting 3D tissue blocks from human body, a vast amount of spatial information (cells and biomarkers) will be derived from various tissue imaging technologies on the tissues (2D and 3D).

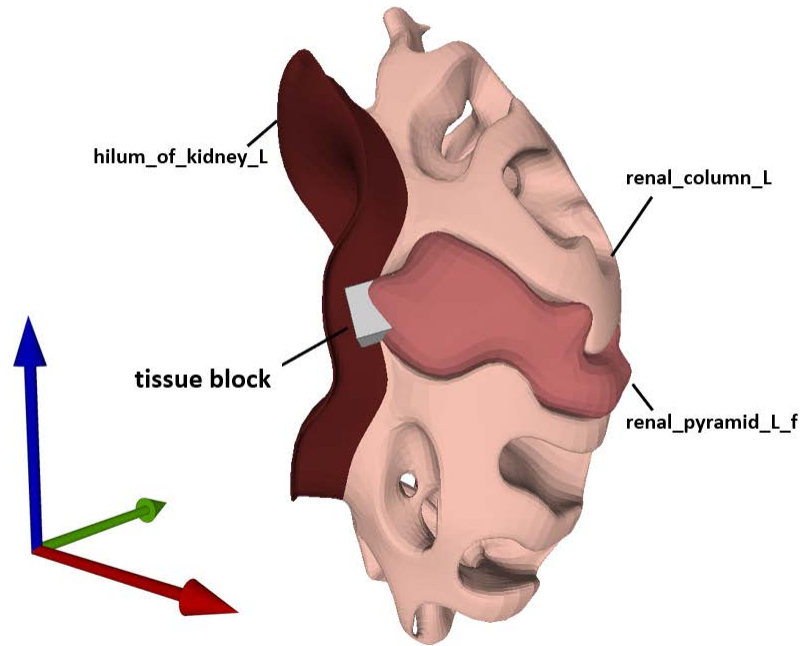


Figure 1: Tissue block registration. The hilum of kidney, renal column and renal pyramid are anatomical structures inside the kidney, which may collide with the tissue block.

An essential component of HuBMAP is tissue block registration [9] (Figure 1), a critical step to enable organ experts to register tissue data to the atlas. It will also help researchers to explore tissue data in a spatially and semantically explicit manner. In order to explore and analyze the inner structures inside the tissue block, 3D computational geometry and spatial data management play a major role for exploring spatial relationships, e.g. anatomical structures that are colliding with the tissue block, as well as quantitative measurements, e.g. volume of each anatomical structure contained in the tissue block. However, there are several challenges we need to address:

Complex 3D Structures: 3D anatomical structures have diverse shapes. Some are in regular shapes while others may have complex structures such as the lung (Figure 2a), kidney (Figure 2b) and brain (Figure 2c). Although the minimal bounding box (MBB) is one of practical approaches to simplify complicated models, MBB is not effective to represent such complex 3D objects for spatial queries. A new indexing method for primitives of 3D models is necessary to reduce the query complexity. Besides, the hierarchical organization of human body demands a multi-level indexing approach.

Varying Mesh Quality of 3D models: 3D models of organs come from different sources such as Allen Brain Atlas [10], the Human Tumor Atlas [11], HuBMAP [6], the Kidney Precision Medicine Project [12] and so on. The mesh quality varies due to different purposes of the projects and varying requirements. For example, visualization oriented 3D organ models are targeted to visualization only, and may have limitations for spatial processing and queries. For instance, there are models with non-manifold edges [13] and

holes, even though smoothness and other post-processing techniques will make the models "look" smooth and perfect. For scientific computing purposes, 3D models for anatomic structures must be spatially compliant to ensure accurate calculation of spatial relationships and measurements. However, it is inevitable to lose vertices or edges due to the occlusion, reflectance or raw data preprocessing, rendering holes in the surface and non-manifold meshes [14]. For example, the mesh in Figure 3a is divided into two parts, i.e., the renal pyramid and the renal papilla, according to biological functionalities and structures. The holes are automatically generated since the surface is not closed any more due to the division of the mesh in Figure 3b. Therefore, a hole filling algorithm needs to be applied to the 3D organ models as Figure 3 shows in advance to guarantee the precision of tissue block registration.

High Computation Complexity: 3D spatial queries involve computationally intensive geometric operations for quantitative measurements and identifications of spatial relationships. While a traditional minimal bounding box approach can filter out the candidates dissatisfying the constraints of spatial queries in the filter stage, the refinement stage still cost too much computation when examining the candidates with respect to their exact geometry to generate the exact solutions [15] [16]. Due to the complex structures of 3D objects, the refinement stage could dominate the spatial query cost. Moreover, queries which require quantitative computations such as intersection volume of objects, have much higher complexity than normal query types.

The above challenges demand a practical and efficient framework that can normalize meshes, exploit indexing techniques suitable for

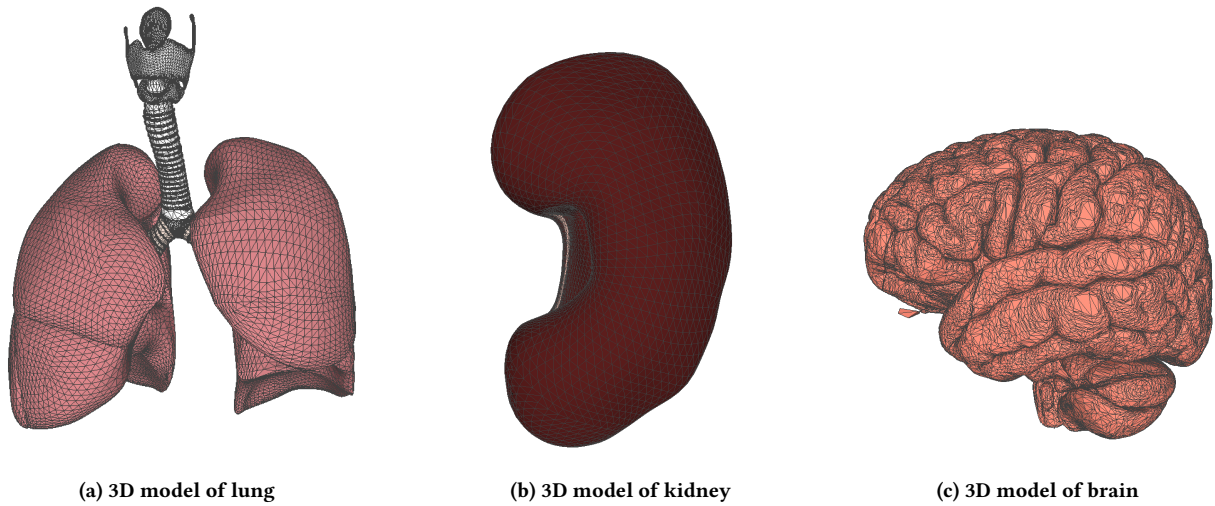


Figure 2: Complex 3D structures

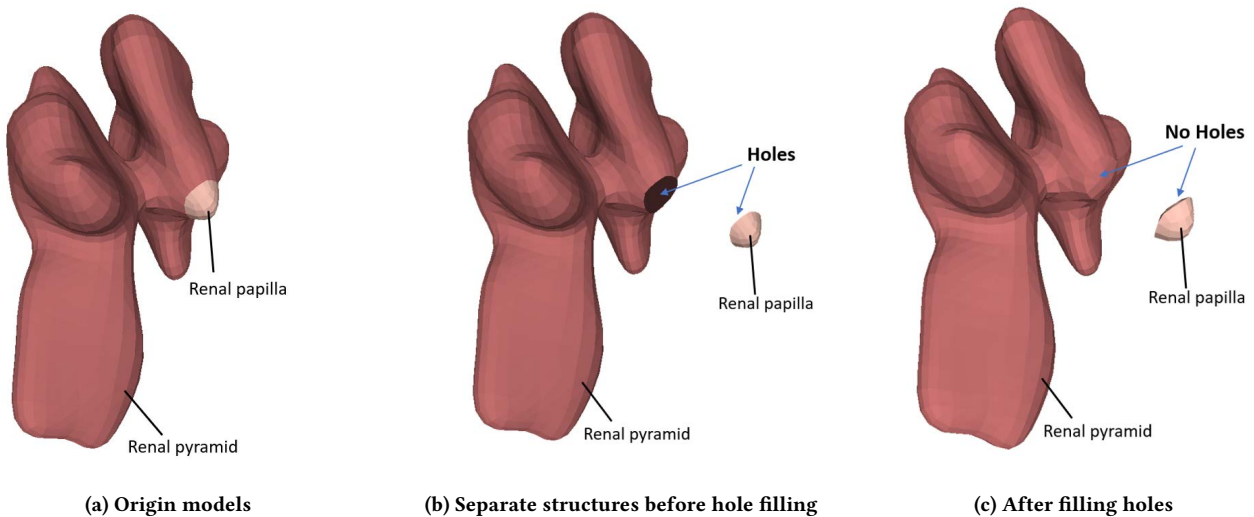


Figure 3: Example of mesh-preprocessing: hole filling

complex objects, reduce computational complexity, and mitigate potential I/O cost to tackle the task of 3D tissue block registration. Our main contributions are summarized as follows:

- We propose a comprehensive framework TICKET for tissue block registration including three steps: (1) Pre-process meshes such as remeshing non-manifold meshes and filling the holes to produce watertight meshes, (2) identify the anatomical structures that are collided with the tissue block, and (3) compute the volume of each anatomical structure contained in the tissue block, if intersected.
- We introduce multi-level spatial indexing at the anatomical structure level and mesh level, which improves query performance compared with the traditional filter-refine paradigm

[17]. We take an in-memory approach for data management to mitigate I/O cost and reduce latency. Besides, we provide a spatial query *http* service for tissue block registration, which can be invoked on-demand when users upload the tissue blocks.

- We develop an efficient voxelization-based method to estimate the intersection volume between the tissue block and the organ considering the regular cuboid shape of the tissue block. We utilize parallel programming to accelerate the volume computation.

The rest of the paper is organized as follows. We first introduce the background in Section 2. The framework of tissue block registration is demonstrated in Section 3. Next, we introduce multi-level

spatial indexing in Section 4. Section 5 presents the voxelization-based method to estimate the intersection volume as well as the parallel computing scheme to accelerate the volume computation. The performance of the framework is evaluated in Section 6. The on-demand spatial query service of tissue block registration is introduced in section 7 followed by conclusion.

2 BACKGROUND

2.1 Mesh Pre-processing

Mesh pre-processing is a fundamental step of 3D data acquisition. Poor quality meshes may cause errors in spatial queries or lead inaccuracy intersection volume computation. There are some typical mesh pre-processing techniques such as mesh self-intersection checking, remeshing and hole filling. Self-intersection checking is intuitive and easy to implement while hole filling is much more subjective and semantic.

Due to the differences of data representation, there are two categories of current hole filling algorithms [14]: point cloud-based methods and mesh-based methods. Point cloud-based methods were developed in earlier years, while mesh-based methods gain more attention and play an important role with the rapid development of computer graphics. Typical workflow of hole filling algorithms can be summarized in two steps: hole boundaries should be first detected and then holes are filled by generating new meshes. In particular, mesh-based hole filling algorithms are divided into two categories: volume-based algorithms and surface-based algorithms according to the data used in the phase of filling holes. In most cases, the simple triangulation algorithms work well to triangulate the polygonal hole regions, especially for the flat and disk-like holes without intense changes to the hole topology and geometry. For large holes that are too complex to fill using triangulation, various hole filling algorithms are proposed [18] [19] [20] [21]. In this paper, we adopt the hole filling algorithm [20] to fill all the problematic holes.

2.2 Spatial Indexing

Each human organ consists of a set of anatomical structures (AS). For example, a kidney has renal pyramids, renal papilla, outer cortex, a total of 35 ASs. A brain contains more than 200 anatomical structures. The organ consisting of multiple ASs is represented by a 3D model, typically using a mesh based representation, using formats such as Graphics Language Transmission Format (e.g., GLB) [22] or Object File Format (OFF) [23]. A typical kidney may be represented by 35 mesh surfaces. To register a human tissue block to an organ, proper indexing is needed for such complex 3D models to minimize the search space and geometric computations. The key principle of the spatial indexing is to divide the search space into regions. There are two common types of space decomposition [24]:

- **Regular decomposition**, also known as space driven index, divides the space in a regular manner independent of the distribution of the objects (i.e., indirectly related to the objects in the space). Objects are mapped to the cells according to some geometric criteria. The most common methods are Quad Tree [25] and cell-based Hashing [26].
- **Object Directed Decomposition** is also known as data driven index. The division of the index space is determined

directly by objects. The space is divided by one of or a combination of the following properties: coordinates of data points, the extents, the bounding box or the spatial objects. The most common examples are K-D tree [27], BSP-tree [28] and R-tree [29]. Although K-D tree and BSP-tree are easier to implement, the deletion and insertion of them are non-trivial while R-tree is designed for dynamic changing data and support deletion and insertion.

Traditional filter-refine paradigm with single spatial index built on MBBs of objects is not suitable for complex objects because the geometric computation during the refinement stage will dominate the spatial query cost. Therefore, building index on primitives (vertices, edges and faces of meshes) can greatly reduce the complexity.

3 OVERVIEW

3.1 Framework of the Tissue Block Registration

We aim to develop a comprehensive framework for tissue block registration, which supports mesh pre-processing, spatial queries on intersection relationship and intersection volume computation. We present the overall framework for the tissue block registration in Figure 4. Initial 3D mesh data is stored in disks in object file format (OFF). We first check whether the meshes are 2-manifold or not. If not, the medical illustrators of HuBMAP will remesh the non-manifold meshes manually. The meshes with holes are then pre-processed by the hole filling algorithm [20]. After the hole filling, the generated patches can be refined and faired [30]. Each individual mesh of anatomical structures will be loaded and stored in memory. We also create a hash map to store the meshes, where the key is the organ name and the value is a list of the meshes of the anatomical structures of the organ for an easy search. Next, an anatomical structure level index will be generated according to the MBBs of the anatomical structures for each organ, and a mesh level index is built for the mesh of every anatomical structure. In addition, different from traditional intersection volume computation based on Boolean Operations [31] on meshes, we propose a voxelization-based method to estimate the intersection volume between the tissue block and the anatomical structure. To accelerate the intersection volume computation, we exploit parallel programming framework OpenMP to check whether each voxel of the tissue block is inside the polygon mesh of the anatomical structure in parallel.

4 MULTI-LEVEL SPATIAL INDEXING

4.1 Anatomical Structure Level Indexing

Figure 1 demonstrates an organ with internal anatomical structures. Different anatomical structures contain different tissue types and cells, with different functionalities. To fast locate the right positions in the organ for the tissue block registration, we build an anatomical structure level index according to the MBBs of the anatomical structures. An R-tree is constructed on the MBBs of the anatomical structures to achieve the dynamic insertion and deletion of the anatomical structures as Figure 5a presents. If cell models are provided in the future, we can further build spatial index on cells [32] based on cell types and spatial distribution patterns. Therefore,

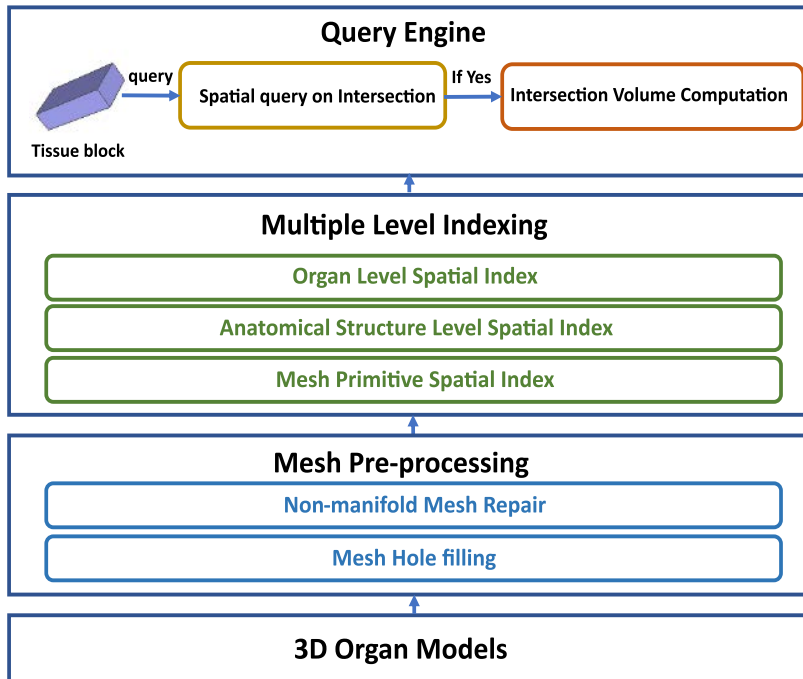


Figure 4: Framework of 3D tissue block registration

from macro level to micro level, we build multi-level spatial indexes according to the hierarchical organisation of our human body.

4.2 Mesh Level Indexing

For complex structures, traditional filter-refine paradigm suffers from geometric computation in the refinement stage, because the simplified MBBs cannot filter out most unqualified candidates, such as a tissue block outside but near the vessel. Therefore, the mesh-level index built on the primitives (faces) of the complicated structure is necessary as Figure 5b. As the resolution of 3D models becomes higher, a mesh-level spatial index can greatly reduce the complexity of spatial queries from $O(N)$ to $O(\log N)$ where N is the number of primitives. Therefore, we build a BSP-tree, also called AABB-tree on the primitives for every static mesh of the anatomical structures.

5 VOXELIZATION-BASED INTERSECTION VOLUME COMPUTATION

The traditional way to compute the intersection volume between two polygon meshes is through Mesh Boolean Operations [31], which consists of two steps: the first step is to compute the mesh intersection of the two polygon meshes. The volume of the intersection mesh is computed next. However, the complexity of Boolean Operations is very high. One of the improvements of Boolean Operations is to use Constructive Solid Geometry (CSG) [33]. Triangle-triangle intersections need to be computed in advance in CSG, which is very time-consuming.

In this paper, we propose an efficient voxelization-based method supporting different resolution of voxelization to estimate the intersection volume. Furthermore, we use the parallel programming framework OpenMP to make the full use of the multi-core processor, which is widely used in modern computers.

5.1 Tissue Representation Transformation

Tissue blocks provided by HuBMAP are described with size, rotation, translation, and scaling parameters, which are not the standard mesh representation by vertices, edges and faces. Therefore, we need to recover the mesh from the parametric representation.

Assuming a tissue block is described as:

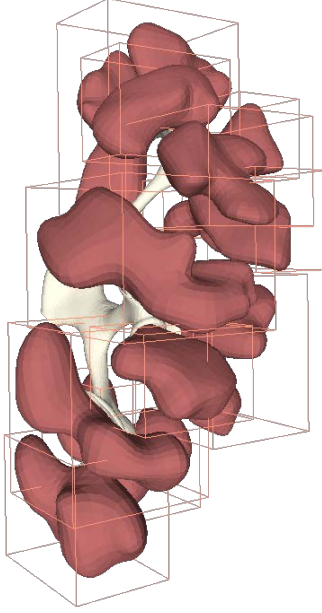
$$\{d_x, d_y, d_z, r_x, r_y, r_z, t_x, t_y, t_z\}$$

where d_x, d_y, d_z are the lengths of the tissue block in x, y, z dimensions respectively, r_x, r_y, r_z are the rotation angles and t_x, t_y, t_z are the translations. The initial center of the tissue block is the origin and the default rotation order is xyz as specified by HuBMAP. Since it is the Euler angle system rather than the fixed angle system that is adopted during rotation by HuBMAP, the rotation order should be adjusted to zyx instead. Hence, the rotation matrix with the rotation angles r_x, r_y, r_z can be written as:

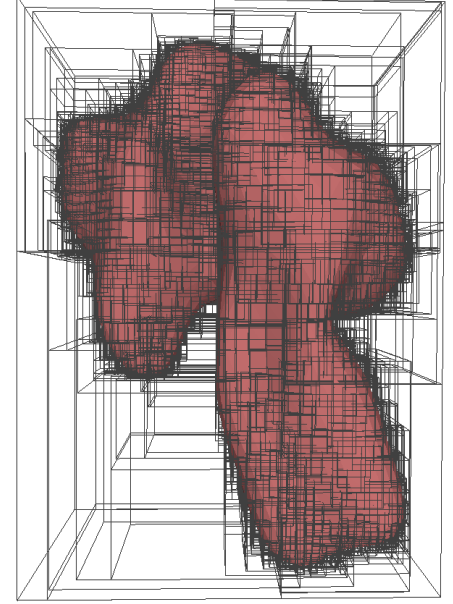
$$R = R_x R_y R_z \quad (1)$$

where

$$R_x = \begin{pmatrix} 1 & 0 & 0 \\ 0 & \cos(r_x) & \sin(r_x) \\ 0 & -\sin(r_x) & \cos(r_x) \end{pmatrix}. \quad (2)$$



(a) Anatomical structure level indexing



(b) Mesh level indexing

Figure 5: Multi-level spatial indexing

$$R_y = \begin{pmatrix} \cos(r_y) & 0 & \sin(r_y) \\ 0 & 1 & 0 \\ -\sin(r_y) & 0 & \cos(r_y) \end{pmatrix}. \quad (3)$$

$$R_z = \begin{pmatrix} \cos(r_z) & \sin(r_z) & 0 \\ -\sin(r_z) & \cos(r_z) & 0 \\ 0 & 0 & 1 \end{pmatrix}. \quad (4)$$

Any point $p = (p_x, p_y, p_z)^T$ inside or on the boundary of the initial tissue block, i.e.,

$$p_x \in \left[-\frac{d_x}{2}, \frac{d_x}{2}\right], \quad (5)$$

$$p_y \in \left[-\frac{d_y}{2}, \frac{d_y}{2}\right], \quad (6)$$

$$p_z \in \left[-\frac{d_z}{2}, \frac{d_z}{2}\right] \quad (7)$$

can be transformed by applying the affine transformation: $p' = Rp + T$ where $T = (t_x, t_y, t_z)^T$, $R = R_x R_y R_z$. Note that the edges and faces relations, the size of the tissue block are not changed due to the affine invariance. Through the above affine transformation, it becomes fairly simple to construct the standard mesh given the initial coordinates of vertices of the tissue block, the rotation matrix and the translation vector.

5.2 Voxelization

A voxel represents a regular grid in 3D space similar to a pixel in a 2D image. Traditionally, voxelization is applied to 3D models in fixed axes directions. Due to regular cuboid shape of the tissue block, we always voxelize the oriented tissue block in its coordinate

system along three different diagonal directions. For each voxel, we test whether the center of the voxel lies inside a certain anatomical structure. The estimated intersection volume can be calculated through the volume sum of the voxels whose center are inside the anatomical structure. Via this approach, the complicated volume computation problem is reduced to a point location test, which saves the computational cost greatly.

Point location test is a very classic problem in computational geometry and the current implementation is based on the number of triangles intersected by a ray with the query point as the source. If the number of triangles intersected is odd, the point is inside the polyhedron. Besides, the AABB tree constructed on each mesh can accelerate the point location queries because the ray casting is an intersection problem essentially. The reuse of AABB trees significantly reduces the overhead. To make the full advantage of multi-core processors, we implement the voxelization-based volume computation in parallel using OpenMP. In addition, to avoid memory overflow, we process the voxelization and point location test on the fly rather than store all the voxels in the memory.

Although the complexity of point location query is $O(\log N)$, a higher resolution voxelization requires more computational resources. We define the resolution coefficient k as the number of voxels in one unit in one dimension, which indicates a tissue block is divided into $kd_x \times kd_y \times kd_z$ voxels. We assume that the lowest resolution is $k = 1$ in which the tissue block is divided into $d_x \times d_y \times d_z$ voxels. Since d_x, d_y, d_z are integers defined by HuBMAP, we can

ignore the "partial" voxel problem. The voxelization-based intersection volume computation algorithm is summarized in Algorithm 1.

Algorithm 1 Parallel computing for voxelization-based volume computation

Input: tissue block t , anatomical structure S
Output: the intersection volume between the tissue block and the anatomical structure

Initialize: $sum \leftarrow 0$
pragma omp parallel for collapse(3) reduction(+:sum)
for i from 1 to kd_x **do**
 for j from 1 to kd_y **do**
 for k from 1 to kd_z **do**
 compute the center c of the voxel located in (i, j, k)
 if c is inside S **then**
 $sum += 1$
 end if
 end for
 end for
end for

return $d_x d_y d_z sum / k^3$

6 EXPERIMENTAL RESULTS

All the tests are conducted on a compute node with a 24-core CPU (AMD Ryzen Threadripper 3960 at 3.8GHz). The node comes with 128GB memory (DDR4 3200) and 2TB SSD (NVMe M.2 PCI-Express 3.0). The OS is Ubuntu 20.04.4 with 5.4.0-124 kernel.

We conduct these tests over the official HuBMAP 3D reference organ models [8] and tissue block dataset [34], which contains 68 tissue blocks registered in kidneys.

First, we compare the loading time of the models and the time of building multi-level spatial indexes for five organ models, namely Kidney, Allen Brain, Lung, Heart and Small Intestine. From Figure 6, we can see that large models such as Allen Brain which contains 282 anatomical structures with total of 324,833 vertices and 656,268 faces, cost more time to load and build spatial indexes while small models such as Small Intestine which contains 9 anatomical structures with total of 16998 vertices and 33524 faces, cost less time to load and build spatial indexes. Besides, building spatial indexes costs only half of the time of loading 3D models to the memory.

Next, we evaluate four different methods (brute force, only building index on MBBs of anatomical structures, only building spatial index on primitives for each mesh, and building multi-level spatial index both on MBBs of anatomical structures and primitives) of the spatial query on intersection. Figure 7 shows the total query time of all 68 tissue blocks of the spatial query on intersection under four different methods. It is obvious that the spatial index on MBBs of ASs, which follows the traditional filter-refine paradigm, can greatly reduce the query time compared with the brute force method. Another important fact is that the spatial index built on primitives can further reduce the query time. We also test the spatial intersection query using PostGIS, which is extremely slow.

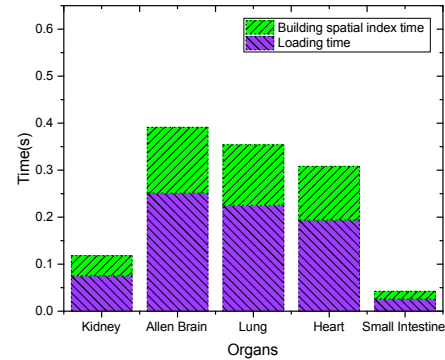


Figure 6: Loading time and building indexes time of different organs

Therefore, the multi-level spatial indexing can significantly improve the performance compared with all other methods.

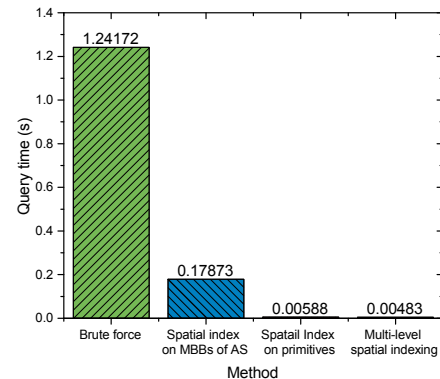


Figure 7: Comparisons of different indexing methods

Moreover, we investigate the impact of parallel computing using OpenMP on voxelization-based intersection volume computation method. From Figure 8 we can conclude that the overhead of cache and synchronization of parallel computing results in no improvement in terms of the query performance when the resolution is low. The number of parallel units increases when the resolution increases. Therefore, the query can make full advantage of multi-core processor, which greatly reduce the query time compared with serial computation.

Finally, we demonstrate the accuracy of the proposed voxelization-based intersection volume computation method. We use the relative error in most cases where the interaction volume exceeds a threshold. Meanwhile, we use the absolute error instead when the intersection volume is around 0. As Figure 9 shows, the error rate decreases as the resolution increases. The error rate is below 0.01 when the resolution is greater than or equal to 8. The outlier with $k = 2$ may be caused by the irregular shape of the 3D models,

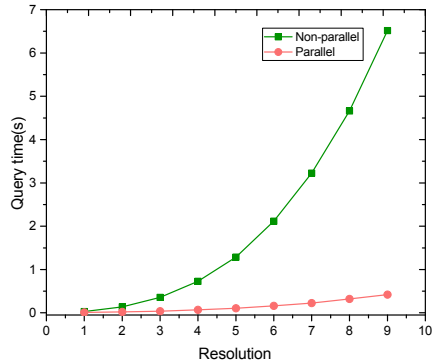


Figure 8: Comparisons of query time between parallel and non-parallel

which seems to have low error rate by accident. In conclusion, the proposed intersection volume computation method achieves high performance in terms of both efficiency and accuracy.

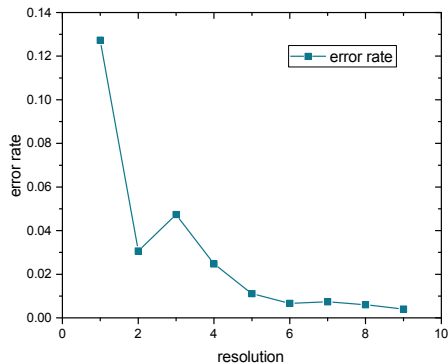


Figure 9: Error rate of different resolutions

7 ON-DEMAND SPATIAL QUERY SERVICE

In this section, we provide an on-demand spatial query *http* service for the ease of use. Users can send a *http* request with the location information of the tissue block including translation, rotation and scaling parameters. The server will process the request accordingly, with the following procedure (the workflow of the tissue registration is also summarized in Algorithm 2): first transform the rotation angle-based representation of the tissue block to a mesh-based representation. Next, the anatomical structures whose MBBs are not overlapped with the MBBs of the tissue block are filtered out by the anatomical structure level index. The exact intersected anatomical structures with the tissue block are reported by using mesh level spatial index. If intersected, we will compute the intersection

volume by proposed voxelization-based intersection volume computation. Otherwise, we will return 0 immediately because they have no intersection.

Algorithm 2 Workflow of tissue block registration

```

for each query for tissue block  $t$  do:
    transform from angle-based to mesh-based representation of
     $t$ ;
    filter with anatomical structure level index;
    query exact intersection with anatomical structures using
    mesh level index.
    if  $t$  is intersected with certain anatomical structure then
        compute the intersection volume using OpenMP specified
        with resolution
    end if
end for

```

8 CONCLUSION

We propose a comprehensive framework for 3D tissue block registration for human atlas. In particular, we build multi-level indexing both on MBBs of anatomical structures and primitives of meshes. In addition, we present a voxelization-based method for intersection volume computation. Experimental results show that the framework achieves high accuracy in real-time spatial queries. The 3D registration framework is implemented as a service for HuBMAP, and will be deployed in Amazon AWS platform for production use in short term future.

9 ACKNOWLEDGMENTS

This research is supported in part by grants from National Institutes of Health 1OT2OD033756-01 and 3OT2OD026671-01S4.

REFERENCES

- [1] Bruce W. Herr II. 2022. Hubmap ccf registration. Retrieved Aug. 30, 2022 from <https://hubmapconsortium.github.io/ccf-ui/rui/>.
- [2] GTEx Consortium Lead analysts: Aguet François 1 Brown Andrew A. 2 3 4 Castel Stephane E. 5 6 Davis Joe R. 7 8 He Yuan 9 Jo Brian 10 Mohammadi Pejman 5 6 Park YoSon 11 Parsana Princy 12 Segrè Ayellet V. 1 Strober Benjamin J. 9 Zappala Zachary 7 8, NIH program management: Addington Anjene 15 Guan Ping 16 Koester Susan 15 Little A. Roger 17 Lockhart Nicole C. 18 Moore Helen M. 16 Rao Abhi 16 Struewing Jeffery P. 19 Volpi Simona 19, Pathology: Sobin Leslie 30 Barcus Mary E. 30 Branton Philip A. 16, NIH Common Fund Nierras Concepcion R. 137, et al. 2017. Genetic effects on gene expression across human tissues. *Nature*, 550, 7675, 204–213.
- [3] Heeva Baharlou, Nicolas P Canete, Anthony L Cunningham, Andrew N Harman, and Ellis Patrick. 2019. Mass cytometry imaging for the study of human diseases—applications and data analysis strategies. *Frontiers in immunology*, 10, 2657.
- [4] Yury Goltsev, Nikolay Samusik, Julia Kennedy-Darling, Salil Bhate, Matthew Hale, Gustavo Vazquez, Sarah Black, and Garry P Nolan. 2018. Deep profiling of mouse splenic architecture with codex multiplexed imaging. *Cell*, 174, 4, 968–981.
- [5] Laura Kuett, Raúl Catena, Alaz Özcan, Alex Plüss, Peter Schraml, Holger Moch, Natalie de Souza, and Bernd Bodenmiller. 2022. Three-dimensional imaging mass cytometry for highly multiplexed molecular and cellular mapping of tissues and the tumor microenvironment. *Nature Cancer*, 3, 1, 122–133.
- [6] Caltech-UW TMC Cai Long leai@caltech. edu 21 b et al. 2019. The human body at cellular resolution: the nih human biomolecular atlas program. *Nature*, 574, 7777, 187–192.
- [7] Katy Börner et al. 2020. Construction and usage of a human body common coordinate framework comprising clinical, semantic, and spatial ontologies. *arXiv preprint arXiv:2007.14474*.

- [8] Bruce W. Herr II. 2022. Ccf 3d reference object library. Retrieved Aug. 30, 2022 from <https://hubmapconsortium.github.io/ccf/pages/ccf-3d-reference-library.html>.
- [9] Katy Borner et al. 2021. Tissue registration and exploration user interfaces in support of a human reference atlas. *bioRxiv*.
- [10] Song-Lin Ding et al. 2016. Comprehensive cellular-resolution atlas of the adult human brain. *Journal of Comparative Neurology*, 524, 16, 3127–3481.
- [11] Sudhir Srivastava et al. 2018. The making of a precancer atlas: promises, challenges, and opportunities. *Trends in Cancer*, 4, 8, 523–536.
- [12] Tarek M El-Achkar et al. 2021. A multimodal and integrated approach to interrogate human kidney biopsies with rigor and reproducibility: guidelines from the kidney precision medicine project. *Physiological genomics*, 53, 1, 1–11.
- [13] Michael Zilske, Hans Lamecker, and Stefan Zachow. 2007. Adaptive remeshing of non-manifold surfaces.
- [14] Xiaoyuan Guo, Jun Xiao, and Ying Wang. 2018. A survey on algorithms of hole filling in 3d surface reconstruction. *The Visual Computer*, 34, 1, 93–103.
- [15] Ablimit Aji, Fusheng Wang, Hoang Vo, Rubao Lee, Qiaoling Liu, Xiaodong Zhang, and Joel Saltz. 2013. Hadoop gis: a high performance spatial data warehousing system over mapreduce. *Proceedings of the VLDB Endowment*, 6, 11, 1009–1020.
- [16] Dejun Teng, Furqan Baig, Hoang Vo, Yanhui Liang, Jun Kong, and Fusheng Wang. 2022. 3dpro: querying complex three-dimensional data with progressive compression and refinement. In *EDBT*, 2–104.
- [17] Shashi Shekhar and Hui Xiong, (Eds.) 2008. *Filter and refine strategy*. *Encyclopedia of GIS*. Springer US, Boston, MA, 320–320. ISBN: 978-0-387-35973-1. DOI: 10.1007/978-0-387-35973-1_415.
- [18] James Davis, Stephen R Marschner, Matt Garr, and Marc Levoy. 2002. Filling holes in complex surfaces using volumetric diffusion. In *Proceedings. First international symposium on 3d data processing visualization and transmission*. IEEE, 428–441.
- [19] Tao Ju. 2004. Robust repair of polygonal models. *ACM Transactions on Graphics (TOG)*, 23, 3, 888–895.
- [20] Peter Liepa. 2003. Filling holes in meshes. In *Proceedings of the 2003 Eurographics/ACM SIGGRAPH symposium on Geometry processing*, 200–205.
- [21] Marco Attene. 2010. A lightweight approach to repairing digitized polygon meshes. *The visual computer*, 26, 11, 1393–1406.
- [22] [SW] The Khronos Group, glTF. URL: <https://www.khronos.org/glTF/>.
- [23] Randi J Rost. 1989. Off-a 3d object file format. *Digital Equipment Corporation Technical Report*.
- [24] Shaik Abdul Nusrath Begum and KP Supreethi. 2018. A survey on spatial indexing. *Journal of Web Development and Web Designing*, 3, 1.
- [25] Hanan Samet. 1984. The quadtree and related hierarchical data structures. *ACM Computing Surveys (CSUR)*, 16, 2, 187–260.
- [26] Ronald Fagin, Jurg Nievergelt, Nicholas Pippenger, and H Raymond Strong. 1979. Extendible hashing—a fast access method for dynamic files. *ACM Transactions on Database Systems (TODS)*, 4, 3, 315–344.
- [27] John T Robinson. 1981. The kdb-tree: a search structure for large multidimensional dynamic indexes. In *Proceedings of the 1981 ACM SIGMOD international conference on Management of data*, 10–18.
- [28] William C Thibault and Bruce F Naylor. 1987. Set operations on polyhedra using binary space partitioning trees. In *Proceedings of the 14th annual conference on Computer graphics and interactive techniques*, 153–162.
- [29] Antonin Guttman. 1984. R-trees: a dynamic index structure for spatial searching. In *Proceedings of the 1984 ACM SIGMOD international conference on Management of data*, 47–57.
- [30] Mario Botsch and Olga Sorkine. 2007. On linear variational surface deformation methods. *IEEE transactions on visualization and computer graphics*, 14, 1, 213–230.
- [31] Aristides AG Requicha and Herbert B Voelcker. 1985. Boolean operations in solid modeling: boundary evaluation and merging algorithms. *Proceedings of the IEEE*, 73, 1, 30–44.
- [32] Yanhui Liang, Hoang Vo, Jun Kong, and Fusheng Wang. 2017. Ispeed: an efficient in-memory based spatial query system for large-scale 3d data with complex structures. In *Proceedings of the 25th ACM SIGSPATIAL International Conference on Advances in Geographic Information Systems*, 1–10.
- [33] Christoph Martin Hoffmann. 1989. Geometric and solid modeling.
- [34] Bruce W. Herr II. 2022. Hubmap ccf exploration. Retrieved Aug. 30, 2022 from <https://portal.hubmapconsortium.org/ccf-eui>.